JKU
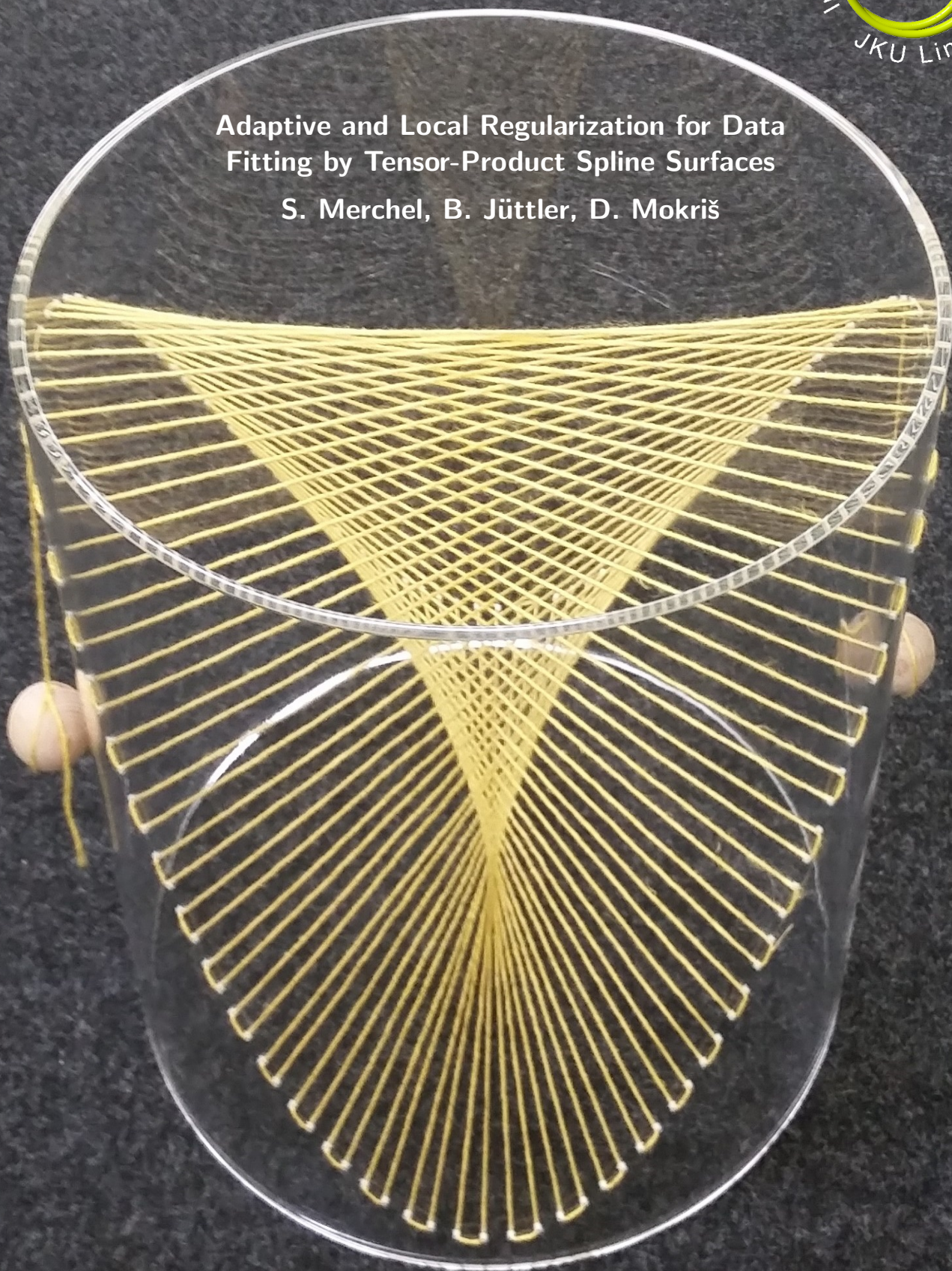
Adaptive and Local Regularization for Data Fitting by Tensor-Product Spline Surfaces

S. Merchel, B. Jüttler, D. Mokriš

Adaptive and Local Regularization for Data Fitting by Tensor-Product Spline Surfaces

S. Merchel · B. Jüttler · D. Mokriš

Abstract We propose to employ a non-constant regularization weight function (RWF) for data fitting via least-squares tensor-product (TP) spline fitting. In the first part of the paper, we formulate the discrete and the continuous version of the problem, and we investigate the influence of the degree of the RWF – which is also chosen as a TP spline function – in the latter situation. The second part presents two methods for automatically generating non-constant RWFs in the discrete situation. These methods are shown to be particularly useful if holes or features are present in the data.

Keywords spline approximation · regularization · data with holes · data with features

Mathematics Subject Classification (2020) MSC 65D07 · MSC 65D10

1 Introduction

Surface fitting is a classical problem in computer-aided geometric design (CAGD). In particular, the need to approximate point data in three-dimensional space arises in several steps of the process of designing and analyzing machine parts, e.g., in order to generate a CAD (Computer-Aided design) model from scanned data.

Several representations of surfaces have been explored in the rich literature on this topic, which include implicit surfaces defined by radial basis functions (Carr et al., 2001) or spline functions (Jüttler and Felis, 2002; Wang et al., 2011),

Sandra Merchel
MTU Aero Engines AG, Dachauer Straße 665, 80995, Munich, Germany
E-mail: sandra.merchel@mtu.de

Bert Jüttler
Institute for Applied Geometry, Johannes Kepler University Linz, Altenberger Straße 69, 4040, Linz, Austria
E-mail: bert.juettler@jku.at

Dominik Mokriš
MTU Aero Engines AG, Dachauer Straße 665, 80995, Munich, Germany
E-mail: dominik.mokris@mtu.de

subdivision surfaces (Hoppe et al., 1994), and parametric spline (or, more generally, NURBS) surfaces (Hoschek and Lasser, 1993; Piegl and Tiller, 1996). We will focus on the latter class of surfaces, which established itself as the universally accepted standard for representing free-form shapes in CAD.

Generating a parametric spline representation typically involves a two-step procedure. The first step is assigning parameter values to the point cloud data and various methods are available for this task, see Floater and Hormann (2005) and the references cited therein. Subsequently, fitting is used to create an approximating surface. Various methods have been investigated in the literature, which include global least-squares fitting (Hoschek and Lasser, 1993), iterative methods (Deng and Lin, 2014; Yang et al., 2004) or spline projection (Bracco et al., 2019). Several authors include the optimization of the parameterization into the fitting (Hoschek, 1988), but this is beyond the scope of the present paper.

We focus on the effects of noisy and uncertain data (in particular with holes) on the least-squares approximation. Regularization is a well-established method (Greiner and Hormann, 1997; Kiss et al., 2014) for handling this type of data. The most common regularization term is the simplified version of the thin plate energy, which is based on the second order partial derivatives of the surface, as in (Hoschek and Jüttler, 1999). Typically, regularization possesses global influence and smooths the resulting surface. Consequently, finding an optimal balance between the quality of the shape and the precision – which is controlled by the choice of the regularization parameter – is of vital interest, cf. (von Golitschek and Schumaker, 1990; von Golitschek and Schumaker, 2002).

While the existing methods perform relatively well for data with a uniform level of noise, they have difficulties if holes or features are present. To address this issue, we propose a novel method that replaces the *constant regularization weight* by a non-negative *regularization weight function (RWF)* acting on the parameter domain. This allows for local control of the regularization.

The remainder of the paper consists of two main parts.

The first part, which is covered by the second section, recalls tensor-product spline functions and introduces least-squares approximation with a non-constant RWF, which is represented by another spline function. We formulate the fitting problem both for the case of continuous and for the case of discrete data. In the first case, we address the case of data that are available on a subdomain only (which is characterized by zero values of the RWF), and we investigate both the uniqueness of the solution and the effect of varying degrees of the RWF.

The second part of the paper, which is contained in Section 3, presents two methods for automatically generating RWFs in the discrete case. The first method uses RWFs with a support-guided choice of the spline coefficients and is particularly well suited for data with holes. The second method uses an error-driven adaptation of the RWF and is especially useful if the data contain features.

These two parts are followed by a conclusion, which summarizes the paper and identifies possible directions for future research.

2 Fitting with regularization

2.1 The two versions of the fitting problem

Given a smooth function $f : \Omega \to \mathbb{R}^n$, where $\Omega = [0,1]^d$ is the unit cube in $\mathbb{R}^d$, we seek for an approximation in a spline space

$$S_h^p = \left\{ \sum_{0 \leq \mathbf{i} \leq \mathbf{m}_h + p} c_{\mathbf{i}} B_{\mathbf{i},h}^p(\mathbf{t}) \mid c_{\mathbf{i}} \in \mathbb{R}^n \right\}, \quad \mathbf{t} = (t_1, \ldots, t_d) \in \Omega,$$

that is spanned by tensor-product B-splines $B_{\mathbf{i},h}^p(\mathbf{t}) = b_{i_1,1,h}^p(t_1) \cdots b_{i_d,d,h}^p(t_d)$ of degree $(p, \ldots, p)$ defined over quasi-uniform knot vectors

$$\Xi_{j,h}^p = (\underbrace{0, \ldots, 0}_{p+1 \text{ times}}, \xi_{1,j,h} \ldots, \xi_{m_{j,h},j,h}, \underbrace{1, \ldots, 1}_{p+1 \text{ times}}), \quad j = 1, \ldots, d,$$

where the lower index h is the mesh size

$$h = \max_{j=1,\ldots,d} \max_{i=0,\ldots,m_{j,h}} \xi_{i+1,j,h} - \xi_{i,j,h}$$

and $\xi_{0,j,h} = 0$ and $\xi_{m_{j,h}+1,j,h} = 1$. In order to guarantee the quasi-uniformity of the knots, we require that

$$\min_{j=1,\ldots,d} \min_{i=0,\ldots,m_{j,h}} \xi_{i+1,j,h} - \xi_{i,j,h} \geq C_{\mathrm{QU}} h$$

is satisfied for some positive constant C_{QU}, which is independent of h. We use multi-indices $\mathbf{i} = (i_1, \ldots, i_d)$ and assume $p > 1$.

Since the n coordinates are dealt with separately, we will restrict the theory to the scalar-valued case $n = 1$. Later we will present examples with $n = 2$ and $n = 3$.

We investigate the influence of regularization when the function f is only available on a subdomain. Our goal is to achieve optimal convergence rate while simultaneously regularizing in the subdomain without data in order to select a sensible solution of an underdetermined problem. We perform regularization based on second derivatives since according to our practical experience it often manages to avoid artifacts such as oscillations and self-intersections. This is essential for applications in CAD since CAD kernels do not accept trimmed surfaces that are constructed from base surfaces possessing self–intersections.

We analyze the spline approximations that are obtained by solving the *regularized fitting problem*

$$\underset{s \in S_h^p}{\text{minimize}} \left(|f - s|_{L^2(\Omega),\omega}^2 + |s|_{W^{2,2}(\Omega),\lambda}^2 \right), \tag{1}$$

where $|\cdot|_{L^2(\Omega),\omega}^2$ is the weighted L^2 seminorm with a non-negative *weight function* ω, which is a norm if ω is positive almost everywhere. In order to keep the presentation simple, we will assume that ω is a piecewise smooth function with a finite number of smooth pieces. Furthermore, we use the weighted $W^{2,2}$ seminorm

$$|s|_{W^{2,2}(\Omega),\lambda} = \left(\int_\Omega \lambda \sum_{\nu=1}^d \sum_{\eta=1}^d (\partial_{\nu\eta} s)^2 \mathrm{d}\mathbf{t} \right)^{\frac{1}{2}},$$

where the non-negative weight function λ is called the *regularization weight function* (RWF). This seminorm is related to the simplified version of the thin-plate energy. Again, we will assume that λ is a piecewise smooth function with a finite number of smooth pieces.

This formulation of the problem is motivated by the approximation of functions that are accessible on a certain closed subdomain $\Omega_0 \subset \Omega$. This is modelled by considering weight functions ω that take value zero on the complementary subdomain $H = \Omega \setminus \Omega_0$, which will be called the *hole*. We will assume that the boundary of H is piecewise smooth with finitely many segments/patches.

It should be noted that the minimum of (1) for $s \in C(\Omega) \cap W^{2,2}(H)$ is not guaranteed to be a highly smooth function. E.g., it is a function that is equal to f on Ω_0 and a linear function on H if $d = 1$ and $\lambda = 0$ on Ω_0. Hence, while the use of regularization may potentially have some benefits for any positive mesh size h, it does not make sense to consider the obtained limit as $h \to 0$.

Clearly, the solution without regularization (i.e., for $\lambda = 0$) is generally not unique if $H \neq \emptyset$, i.e., several spline approximations that realize the smallest value of the objective function exist for sufficiently small mesh size h. Note that ω is bounded since we consider it as a function on the unit cube Ω, which is a compact subset of $\mathbb{R}^d$. Consequently, the L^2 norm can be used to bound the weighted L^2 seminorm,

$$|\phi|_{L^2(\Omega),\omega} \leq \|\omega\|_{L^\infty(\Omega)} \|\phi\|_{L^2(\Omega)} .$$

This observation implies the following result:

Lemma 1 *If $\lambda = 0$ and $f \in W^{p+1,2}(\Omega)$ with $p + 1 > d/2$, then any solution s_h of* (1) *satisfies*

$$|f - s_h|_{L^2(\Omega),\omega} \leq C_0 h^{p+1} ,$$

where C_0 is independent of h, but depends on C_{QU}, f, ω and p.

This result follows directly from classical results from spline theory (de Boor and Fix, 1973), which ensure the existence of quasi-interpolation operators Π_h^p that transform any given function $\phi \in W^{p+1,2}(\Omega)$ into a spline function $\Pi_h^p \phi$. We may express these operators as

$$\Pi_h^p : W^{p+1,2}(\Omega) \to S_h^p , \ \ \phi \mapsto \Pi_h^p(\phi) = \sum_{0 \leq \mathbf{i} \leq \mathbf{m}_h + p} B_{\mathbf{i},h}^p(\mathbf{t}) \mu_{\mathbf{i},h}^p(\phi)$$

with linear coefficient functionals $\mu_{\mathbf{i},h}^p$. According to a classical result (de Boor and Fix, 1973, Theorem 5.2 with $\ell = q = 0$ and $r = 2$), the error satisfies

$$\|\phi - \Pi_h^p \phi\|_{L^2(\Omega)} \leq C_1 h^k |\phi|_{W^{k,2}(\Omega)} \tag{2}$$

for $1 \leq k \leq p + 1$. The constant C_1 is independent of $\Xi_{j,h}^p$ and h, but it depends on C_{QU}. The case $k = p + 1$ is needed to derive the Lemma, while $k = 1$ will be used to establish a (pointwise) convergence property of the coefficient functionals in the appendix.

Two cases of weight functions ω will be analyzed in the remainder of the paper:

1. The weight function ω is a classical function (as opposed to the next case) that is zero on the hole $H \subset \Omega$. This is considered in the next section and suitable choices of the RWF λ are analyzed.

2. We also consider generalized weight functions ω which are sums of Dirac delta functions

$$\omega(\mathbf{t}) = \frac{1}{N} \sum_{i=1}^{N} \delta(\mathbf{t} - \mathbf{t}_i)$$

for a finite set of nodes $\mathbf{t}_i \in \Omega$. This transforms Problem (1) into the *discrete fitting problem*

$$\underset{s \in S_h^p}{\text{minimize}} \left(\frac{1}{N} \sum_{i=1}^{N} \|f(\mathbf{t}_i) - s(\mathbf{t}_i)\|^2 + |s|_{W^{2,2}(\Omega),\lambda}^2 \right) . \tag{3}$$

Lemma 1 does not apply, since ω is not a classical function. However, the original problem can be seen as the limit case of the discrete version as $N \to \infty$. We will return to this problem in Sections 3.1 and 3.2.

2.2 Regularization with optimal rate of convergence

We consider a classical weight function ω which is equal to zero on the hole $H \subset \Omega$. We investigate the influence of the regularization weight function. In contrast to the non-uniqueness of the solutions to the unregularized problem, i.e., $\lambda = 0$ on Ω, the regularized problem (1) possesses a unique solution under a mild assumption on the RWF:

Lemma 2 *The solution of Problem* (1) *is unique if the regularization weight function* $\lambda + \omega$ *is positive almost everywhere and* $\|\omega\|_{L^2(\Omega)} \neq 0$.

Proof Since $\lambda + \omega$ is positive almost everywhere we have $\text{supp}(\lambda) \cup \text{supp}(\omega) = \Omega$. (Note that we use the closed support of a function, and not the set-theoretic one.) The regularized fitting problem defines the non-negative definite quadratic form

$$Q(s) = |s|_{L^2(\Omega),\omega}^2 + |s|_{W^{2,2}(\Omega),\lambda}^2 \text{ on } S_h^p .$$

It is positive definite since $Q(s) = 0$ implies that

$$|s|_{L^2(\Omega),\omega}^2 = 0 \text{ and } |s|_{W^{2,2}(\Omega),\lambda}^2 = 0 ,$$

hence $s = 0$ on $\text{supp}\,\omega$, which has a non-empty interior as ω is assumed to be a piecewise smooth function with a finite number of smooth pieces. Moreover, s is linear on $\text{supp}\,\lambda$, thus $s = 0$ on the entire domain $\Omega = [0,1]^d$, due to $p > 1$ and $\text{supp}(\lambda) \cup \text{supp}(\omega) = \Omega$.

Consequently, when considering the representation of the unknown function s with respect to the B-splines spanning S_h^p, Problem (1) is equivalent to the minimization of a quadratic function on the coefficient space. The solution is unique since the quadratic form assigns the zero value to the difference of any two minimizers s and $\hat{s}$. □

Next, we analyze the error of this unique solution. We will assume that the RWF λ fulfils the condition

$$\lambda(\mathbf{t}) \begin{cases} = 0 & \text{if } \mathbf{t} \notin H , \\ \leq \varepsilon \operatorname{dist}(\mathbf{t}, \partial H)^q & \text{otherwise} \end{cases} \tag{4}$$

for some constant $\varepsilon > 0$ and for some degree q, and is positive on the hole H, which is a subdomain. Consequently, the RWF satisfies the assumptions of Lemma 2. In practice, one would first construct λ and check that there exists a ε satisfying (4); the ε then appears in the following estimate. Note that it can be modified simply by multiplying λ with a positive constant.

Theorem 1 *The solution s_h of (1) satisfies*

$$|f - s_h|^2_{L^2(\Omega),\omega} \leq C_2(1+\varepsilon)h^{2p+2} \; ,$$

if λ satisfies (4) and the degree q of λ fulfils $q \geq 2p+4+d$, where the constant C_2 depends on f, ω, p and q.

Proof We define the truncation operator $T^p_h : S^p_h \to S^p_h$ as

$$T^p_h \left(\sum_{0 \leq \mathbf{i} \leq \mathbf{m}_h+p} \mathbf{c_i} B^p_{\mathbf{i},h}(\mathbf{t}) \right) = \sum_{\substack{0 \leq \mathbf{i} \leq \mathbf{m}_h+p, \\ B^p_{\mathbf{i},h}|_{\Omega_0} \neq 0}} \mathbf{c_i} B^p_{\mathbf{i},h}(\mathbf{t}) \; .$$

We generate a spline approximation of f with the help of the quasi-interpolation operator Π^p_h and the truncation operator T^p_h,

$$u_h = T^p_h \Pi^p_h f \; . \tag{5}$$

Now, we consider the solution $s_h \in S^p_h$ to Problem (1) and obtain

$$\begin{aligned}
|f - s_h|^2_{L^2(\Omega),\omega} &\leq |f - s_h|^2_{L^2(\Omega),\omega} + |s_h|^2_{W^{2,2}(\Omega),\lambda} \\
&\leq \underbrace{|f - u_h|^2_{L^2(\Omega),\omega}}_{(i)} + \underbrace{|u_h|^2_{W^{2,2}(\Omega),\lambda}}_{(ii)} \leq C_2(1+\varepsilon)h^{2p+2} \; ,
\end{aligned}$$

with $C_2 = \max(C_1^2 \|\omega\|^2_{L^\infty(\Omega)} \|f\|^2_{W^{p+1,2}(\Omega)}, C_3)$, where we used the approximation properties (2) of the quasi-interpolation operator, together with the observation

$$T^p_h(\Pi^p_h f)|_{\Omega_0} = \Pi^p_h f|_{\Omega_0}$$

and Proposition 1 (see Appendix) to estimate the two terms (i) and (ii), respectively. □
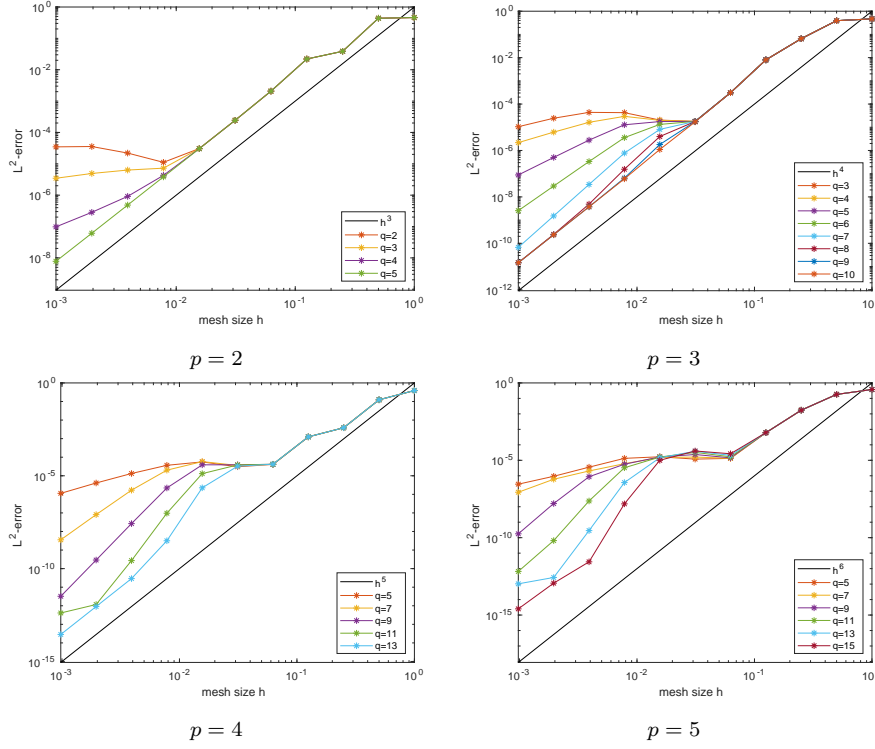
We conclude the section with some numerical results. In the following examples we will choose $\lambda \in S^q_k$ as a spline function

$$\lambda(\mathbf{t}) = 10^{-6} \sum_{\substack{0 \leq \mathbf{i} \leq \mathbf{m}_k+q, \\ B^q_{\mathbf{i},k}|_{\Omega_0}=0}} B^q_{\mathbf{i},k}(\mathbf{t}) \; ,$$

with a uniform knot vector of mesh size $k = \frac{1}{128}$.

First, we present a univariate example to illustrate the observations of Theorem 1. We solve Problem (1) for

$$f(t) = \sin(4\pi(t + \frac{1}{80})) \; ,$$

Fig. 1 Univariate example: Rate of convergence of the regularized approximation for $p = 2, 3, 4, 5$ and various values of the degree q.

with $\Omega = [-1, 1]$ and $H = [-\frac{1}{2}, \frac{1}{2}]$, using splines of degree $p = 2, \ldots 5$ with dyadically refined uniform knots (starting with $h = 1$), and for various degrees of the RWF. The results are reported in Figure 1. According to Theorem 1, choosing $q \geq 2p + 5$ would ensure the optimum rate of convergence. The experimental results confirm the theoretical bound, but we already get good results for smaller degrees q.

Unfortunately, the condition number of the linear system obtained from Problem 1 becomes rather high as h decreases, especially for higher values of the degree q. Figure 2 reports these condition numbers for the univariate example for various combinations of p and q. For comparison we also plot the condition number for a constant regularization as a baseline.

Very high condition numbers lead to numerical solutions with artifacts, especially near the boundary of the hole. In practice, one may use lower values of q and accept that Theorem 1 – which states a sufficient condition anyway – cannot be applied. For instance, using $q = 7$ for cubic splines does not increase the condition number too much compared to the constant regularization, but still gives good approximation results. Alternatively, it is also possible to employ advanced stabilization techniques as described in Chu et al. (2022), which should improve the situation.

$p = 2$

$p = 3$

$p = 4$

$p = 5$
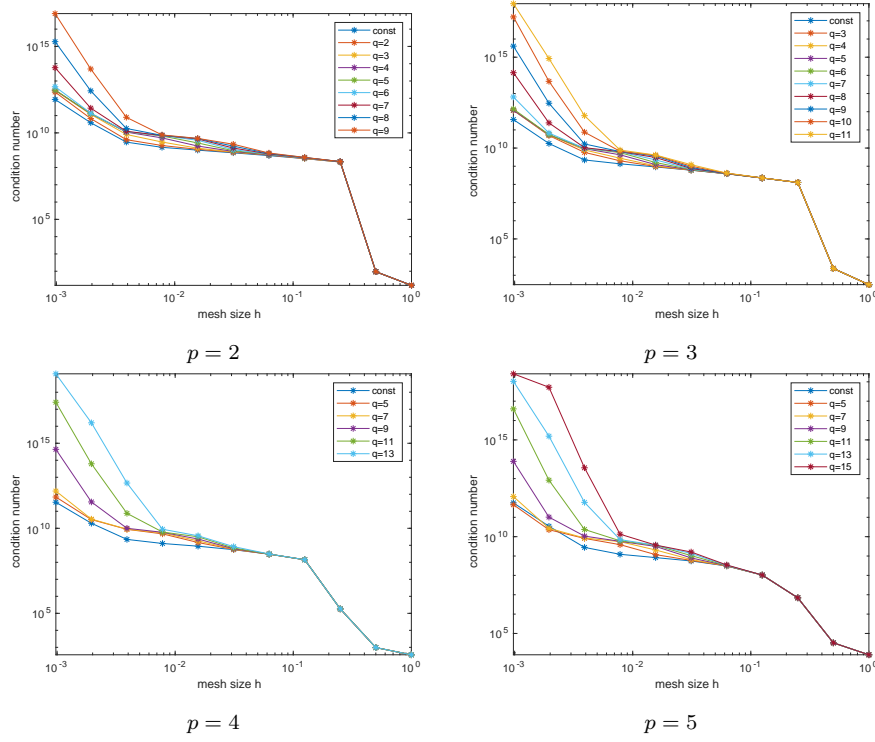
Fig. 2 Univariate example: Condition numbers for $p = 2, 3, 4, 5$ and various values of the degree q.

Second, we consider the bivariate case in order to illustrate that the theory applies to this situation also. More precisely, we solve Problem (1) for

$$f(t_1, t_2) = \sin(4\pi(t_1 + \frac{1}{80})) \sin(4\pi(t_2 + \frac{1}{80})) \, ,$$

with $\Omega = [-1, 1]^2$ and $H = [0, 1]^2$, using splines of degree $p = 2, \ldots 5$ with dyadically refined uniform knots (starting with $h = 1$), and for various degrees of the RWF. The results are reported in Figure 3. According to Theorem 1, choosing $q \geq 2p + 6$ would ensure the optimum rate of convergence. The experimental results indicate a good agreement with the theoretical bound. As before, even smaller degrees q already give good results.

3 Data-dependent RWFs in the discrete case

In the remainder of the paper, we will address the discrete fitting problem (3) (i.e., the case of weight functions ω that are sums of Dirac delta functions), due to its practical importance. The given data thus consists of a set of values

$$f_i = f(\mathbf{t}_i)$$
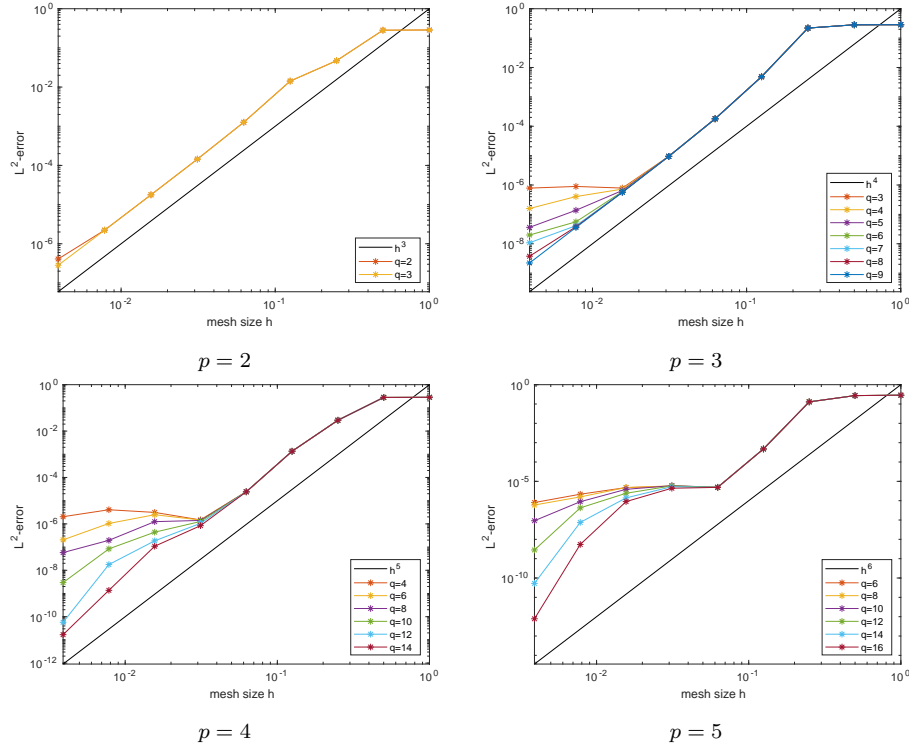
Fig. 3 Bivariate example: Rate of convergence of the regularized approximation for $p = 2, 3, 4, 5$ and various values of the degree q.

with associated parameters t_i, $i = 1, \ldots, N$, which we collect in the set

$$T = \{\mathbf{t}_j, \ j = 1, \ldots, N\} .$$

The theoretical results from the previous section are no longer applicable for the discrete problem. Nevertheless, our goal of using regularization is very similar; we want to achieve good accuracy while regularizing in order to avoid artifacts. Therefore, we try to apply an analogous setting in the discrete case.

We will propose two methods that adapt the RWF λ to the given data. Both generate RWFs $\lambda \in S_k^q$, which are spline functions

$$\lambda(\mathbf{t}) = \sum_{0 \leq \mathbf{i} \leq \mathbf{m}_k + q} \lambda_{\mathbf{i}} B_{\mathbf{i}, k}^q(\mathbf{t}) \tag{6}$$

of some degree q with RWF mesh size k.

3.1 On-Off regularization

The first method is particularly suited if the data contains *holes*, i.e., if large regions without any data are present. The choice of the RWF degree is guided by the experimental results from the previous section. We assume that the RWF

mesh size k exceeds the sampling density but is still much smaller than the hole size.

We propose a *support-guided construction* of the RWF λ. Given two constants $\lambda_{\max} > \lambda_{\min} > 0$, we chose the coefficients in (6) as

$$\lambda_{\mathbf{i}} = \begin{cases} \lambda_{\max} & \text{if} \quad \forall j : B_{\mathbf{i},k}^q(\mathbf{t}_j) = 0 \ , \\ \lambda_{\min} & \text{otherwise} \ . \end{cases} \tag{7}$$

We present two examples.

The *first example*, which uses artificially generated data, shows that the support-guided adaptation method of the RWF may give better results than constant regularization. In the example we solve Problem (1) for data which are sampled from the surface in Figure 4.
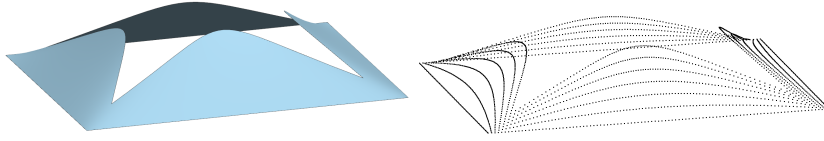
Fig. 4 Input surface and the sampled points.

The surface is constructed from the cubic Bézier surface with control points

$$\mathbf{c}_{0,0} = (0,0,0)^T, \quad \mathbf{c}_{0,1} = (1,0,0)^T, \quad \mathbf{c}_{0,2} = (2,0,0)^T, \quad \mathbf{c}_{0,3} = (3,0,0)^T,$$
$$\mathbf{c}_{1,0} = (0,1,0)^T, \quad \mathbf{c}_{1,1} = (6,6,4)^T, \quad \mathbf{c}_{1,2} = (-3,6,4)^T, \quad \mathbf{c}_{1,3} = (3,1,0)^T,$$
$$\mathbf{c}_{2,0} = (0,2,0)^T, \quad \mathbf{c}_{2,1} = (6,-3,4)^T, \quad \mathbf{c}_{2,2} = (-3,-3,4)^T, \quad \mathbf{c}_{2,3} = (3,2,0)^T,$$
$$\mathbf{c}_{3,0} = (0,3,0)^T, \quad \mathbf{c}_{3,1} = (1,3,0)^T, \quad \mathbf{c}_{3,2} = (2,3,0)^T, \quad \mathbf{c}_{3,3} = (3,3,0)^T.$$

This surface is trimmed in the parameter domain by the rectangle $]0.5, 0, 95[\times]0.6, 0.95[$, which corresponds to the hole for this example. We sample the surface on a regular grid with mesh size $\frac{1}{100}$.

The data are fitted with a B-Spline tensor-product surface of degree $p = 3$ and with mesh size $h = 0.0625$. A regularization is needed since choosing $\lambda = 0$ leads to infinitely many solutions. We show in Figure 5 the approximations using the support guided construction (7) of the RWF with $k = 0.01875$ and $q = 12$ for various values of $\lambda_{\min}$ and $\lambda_{\max}$.

The standard method of using a *constant* RWF is equivalent to choosing $\lambda_{\min} = \lambda_{\max}$; this corresponds to the diagonal elements in the upper part (above the dashed line) of Figure 5. Clearly, a rather large regularization is needed to avoid self-intersections. Such a choice of the RWF, however, entails a large approximation error, as one may see by comparing the original straight patch boundaries in Figure 4 with their curved approximations in Figure 5 ($\lambda_{\min} = \lambda_{\max} = 10^{-1}$) or by comparing the errors in Table 1. Choosing smaller values of the constant RWF leads to approximations with self-intersections, see Figure 5 ($\lambda_{\min} = \lambda_{\max} = 10^{-4}$ and 10^{-7}). While we obtain a good fit of the data and a good approximation error, see Table 1, the surface is still unsuitable for applications, as one may encounter difficulties when using it as a base surface for a trimmed surface patch.

λ_{max} / λ_{min}	10^{-1}	10^{-4}	10^{-7}
10^{-1}	$2.78e{-}1$ / $6.54e{-}2$	$2.13e{-}1$ / $5.16e{-}2$	$2.12e{-}1$ / $5.15e{-}2$
10^{-4}	$2.86e{-}2$ / $3.91e{-}3$	$6.32e{-}3$ / $6.61e{-}4$	$6.32e{-}3$ / $9.32e{-}4$
10^{-7}	$3.14e{-}2$ / $4.31e{-}3$	$2.72e{-}3$ / $6.12e{-}4$	$1.42e{-}5$ / $3.75e{-}6$
0	$3.14e{-}2$ / $4.31e{-}3$	$2.74e{-}3$ / $6.17e{-}4$	$1.05e{-}6$ / $2.06e{-}6$

Table 1 First example: L^∞/L^2-errors of the approximations for various values of λ_{min}, λ_{max}.
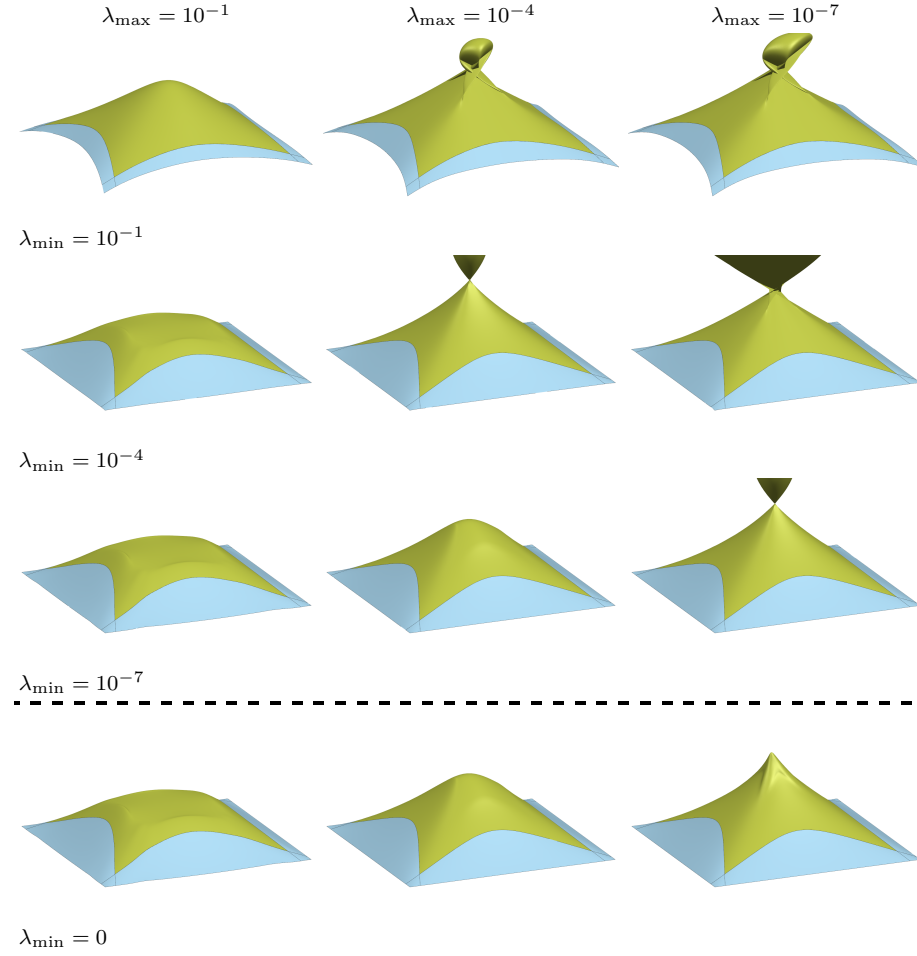
Fig. 5 First example: Results obtained for support-guided RWFs with various values of λ_{min} (rows) and λ_{max} (columns).

$\lambda = 10^{-5}$	$\lambda = 10^{-7}$	support-guided RWF
$1.88e{-}5$ / $2.87e{-}6$	$1.69e{-}5$ / $2.75e{-}6$	$1.69e{-}5$ / $2.83e{-}6$

Table 2 Second example: ME / RMSE of the approximations of the endwall

The self-intersection is still present for approximations with support-guided construction (7) of the RWF for $\lambda_{\min} > \lambda_{\max}$, whereas they disappear in the cases $\lambda_{\min} < \lambda_{\max}$, see Figure 5. For the cases without self-intersection $\lambda_{\max}$ influences the behaviour of the approximation in the hole. It seems that choosing $\lambda_{\max} = 10^{-4}$, $\lambda_{\min} = 10^{-7}$ or 0 is a good trade-off between accuracy and quality of the approximation, see Figure 5 and Table 1.

In practice, the determination of the optimal choice of $\lambda_{\min}$ and $\lambda_{\max}$ might not be straight-forward and depends on the specific example. In general, we suggest to use $\lambda_{\min} < \lambda_{\max}$, where $\lambda_{\min}$ should be chosen according to the type of data given on $\Omega \setminus H$. For example, if the data contains noise, a certain minimal value of $\lambda_{\min}$ might be required to avoid oscillations with respect to the data; at the same time, $\lambda_{\min}$ should not be too high in order to keep the error low. The choice of $\lambda_{\max}$ depends on the desired behaviour within the hole. Therefore, a user-guided choice is suggested.

As the *second example*, we reconstruct the surface of a turbine endwall, see Figure 6 (a), where the measured data consisting of $109,965$ samples have a hole at the connection to the turbine blade, see Figure 6 (b).
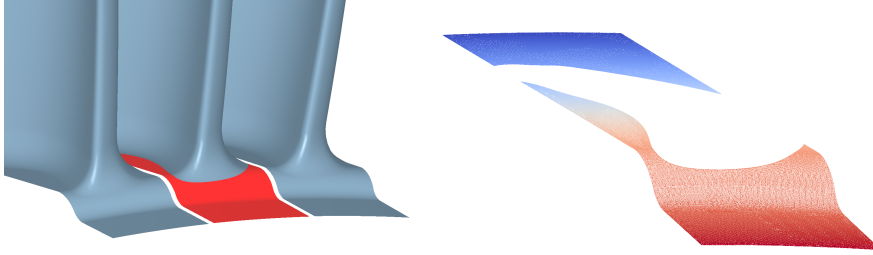

Fig. 6 Second example: Turbine endwall (red, left) and input points (coloured according to the u-parameter, right).

We compare two results of the classical method with constant regularization parameters $\lambda = 10^{-5}$ and $\lambda = 10^{-7}$ with the support-guided construction of the RWF with $\lambda_{\max} = 10^{-5}, \lambda_{\min} = 10^{-7}$. In all three cases we used cubic tensor-product B-splines with $1,273$ degrees of freedom. The results are shown in Figure 7.

While all the results have a comparable root mean square error (RMSE) and maximum error (ME), see Table 2, the advantage of the support-guided RWF becomes clear when considering the approximation close to and inside the hole. Approximation with constant regularization produces an artifact in the form of a bump where no data is provided, see Figure 7. This artifact makes the result unsuitable for the subsequent geometric processing, in particular concerning the construction of blend surfaces via the rolling ball method.

This problem is no longer present for the third approximation. We generate a support-guided RWF according to (7) with $k = 0.015625$ and degree $q = 3$. Even if this degree is lower than the ones considered in the previous section, it works well in practice and speeds up the computation since fewer Gauss nodes are needed and a larger value of k is sufficient to achieve the desired effect. Summing up, we obtain a better approximation since the resulting surface is as flat as the input data, thus adhering to user expectation.
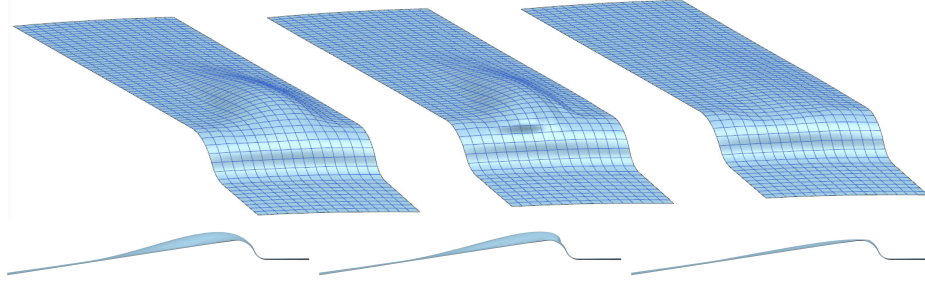
Fig. 7 Approximations (top row), and side view of the approximation (bottom row) obtained for a constant RWF $\lambda = 10^{-5}$ (left), another constant RWF $\lambda = 10^{-7}$ (center) and the support-guided RWF (right) with $\lambda_{\max} = 10^{-5}, \lambda_{\min} = 10^{-7}$.

As demonstrated by the two examples, the support-guided approach works well for data with holes. However, it is not yet suitable for data with varying sampling density. A more general approach will be described in the next section.

3.2 Bounded slope regularization

We present an iterative method that generates a RWF of degree 0, based on the distribution of the fitting error.

1. Given a relatively large regularization parameter $\lambda^{(0)}$, we solve the regularized fitting problem for $\lambda(\mathbf{t}) = \lambda^{(0)}$, i.e., for a RWF with coefficients $\lambda_{\mathbf{i}} = \lambda^{(0)}$.
2. We apply Algorithm 1 in order to modify the coefficients $\lambda_{\mathbf{i}}$. More precisely, we decrease the values $\lambda(\mathbf{t}_j)$ of the RWF if the error at t_j exceeds a given threshold ε, i.e., if
$$||s_h(\mathbf{t}_j) - f_j|| \geq \varepsilon.$$
Simultaneously, we keep the discrete logarithmic slope of the RWF bounded,
$$\lambda_{\mathbf{j}}/\lambda_{\mathbf{i}} \geq \alpha^k \quad \text{if} \quad |\mathbf{i} - \mathbf{j}| \leq 1 \ ,$$
where the user-defined constant $\alpha < 1$ specifies the maximum discrete logarithmic slope and k is the mesh size of the RWF.
3. We solve the regularized fitting problem for the modified RWF and continue with the previous step, or we abandon the procedure if the RWF did not change or if a maximum number of iterations has been reached. The maximum number of iterations is chosen as
$$\left\lfloor \frac{\log(\lambda_{\min}) - \log(\lambda^0)}{\log(\alpha^k)} \right\rfloor \tag{8}$$

since this ensures that the minimum of the RWF coefficients $\lambda_{\mathbf{i}}$ does not get smaller than $\lambda_{\min}$.

Algorithm 1: Adaptive (error-driven) choice of the RWF

Input : coefficients $\lambda_{\mathbf{i}}$ of the RWF and regularized spline approximation s_h
Output: modified coefficients $\lambda_{\mathbf{i}}$, adapted according to the error distribution

```
1 for i = 0, ..., mₖ do
2 |   for j = 1, ..., N do
3 |   |   if B⁰_{i,k}(tⱼ) ≠ 0 and ‖sₕ(tⱼ) − fⱼ‖ > ε then
4 |   |   |   λᵢ ← λᵢ · αᵏ;
5 |   |   |   break /*   exit loop for j                              */
6 chc ← true /*   chc = ''coefficient has changed''                  */
7 while chc do
8 |   chc ← false;
9 |   for i, j = 0, ..., mₖ do
10 |   |   if |i − j| = 1 and λⱼ/λᵢ < αᵏ then
11 |   |   |   λᵢ ← λᵢ · αᵏ;
12 |   |   |   chc ← true
```


Again we present two examples.

The *first example*, which is again based on artificially generated data, explores the influence of the RWF mesh size k and the slope parameter α, focusing on the univariate case. We consider a set of data $(t_i, f_i)_{i=0,\ldots,43} \in \mathbb{R}^2$, see Figure 8. It combines relatively dense data from the graph of a scaled trigonometric function on the right-hand side with sparse data from a straight line on the left-hand side. The figure depicts the B-spline approximations in $S^3_{1/36}$ obtained by solving problem (3) for various constant RWFs. In addition, we visualize the curvature by plotting the graph of the signed logarithm

$$\text{sign}(s_h'') \log(1 + |s_h''|)$$

of the second derivative.

$\lambda = 10^{-2}$ $\lambda = 10^{-6}$ $\lambda = 10^{-10}$
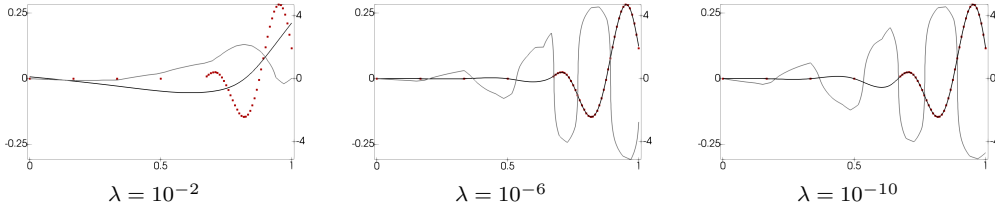
Fig. 8 B-Spline approximations of a univariate data set (visualized as red squares) for various constant RWFs. The grey curve – which refers to the axis on the right–hand side – represents the signed logarithm of the second derivative.

We observe that the constant RWF does not give good results. We either obtain large oscillations for small constant values of the RWF or big errors for large constant values of the RWF, see Figure 8 and Table 3.

Constant λ			
$\lambda = 10^{-2}$	$\lambda = 10^{-6}$	$\lambda = 10^{-10}$	$\lambda = 10^{-14}$
$1.48e{-}1$ / $5.95e{-}2$	$6.87e{-}3$ / $8.84e{-}4$	$8.57e{-}5$ / $2.61e{-}5$	$8.58e{-}5$ / $2.61e{-}5$
λ from RWF adaptation algorithm			
	$\alpha = 10^{-\frac{5}{2}}$	$\alpha = 10^{-10}$	$\alpha = 10^{-40}$
$k = \frac{1}{5}$	$4.94e{-}4$ / $1.48e{-}4$	$2.46e{-}4$ / $8.05e{-}5$	$8.57e{-}5$ / $2.61e{-}5$
$k = \frac{1}{20}$	$8.31e{-}4$ / $2.57e{-}4$	$8.42e{-}4$ / $3.10e{-}4$	$7.55e{-}4$ / $2.73e{-}4$
$k = \frac{1}{80}$	$9.81e{-}4$ / $3.19e{-}4$	$9.60e{-}4$ / $3.90e{-}4$	$9.96e{-}4$ / $2.86e{-}4$

Table 3 L^{∞}/L^{2}-errors of the curves discussed in the first example

Now we use the error-guided RWF adaptation (see Algorithm 1) to create different non-constant RWFs λ. The procedure is initialized with a constant RWF $\lambda \in S_k^0$, which is equal to $\lambda^{(0)} = 10^{-2}$ on the entire domain. We then alternate between solving the regularized fitting problem and applying Algorithm 1 with $\varepsilon = 10^{-3}$ until we reach the maximum number (8) of iterations, where $\lambda_{\min} = 10^{-10}$.

Figure 9 depicts the automatically generated RWFs and the resulting approximations, respectively, for various values of the RWF mesh size k and of the constant α that specifies the maximum discrete logarithmic slope of the RWF. We note that for the same values of α the slope of the corresponding RWFs is approximately the same for small enough values of k. We conclude the choice of k has little influence, provided that it is sufficiently small.

Visual inspection indicates that we get best results for smaller values of both α and h, which correspond to the lower right part of the second figure. Clearly, the possibility to decrease these parameters is limited by the precision of the floating point numbers.

Table 3 reports the L^{∞}-error and L^{2}-error of the approximations. We note that the errors obtained by the adaptive method all possess the same order of magnitude, while the constant regularization needs low values of the regularization parameter to match these results.

In the *second example*, we apply the method of data obtained from an optical scan of a turbine blade. The input is a parameterized triangle mesh with $271,914$ vertices. The data are approximated by solving the discrete regularized fitting problem (3) for cubic tensor-product B-Splines with $27,191$ degrees of freedom.

We compare the results obtained for two constant values of the RWF λ, and for a piecewise constant RWF with $k = 0.015625$, see Figure 10, which is automatically generated by the error-guided adaptation algorithm with $\varepsilon = 5 \cdot 10^{-5}$ and $\alpha = 10^{-10}$. The procedure is initialized with $\lambda = 10^{-4}$.

The figure visualizes the distribution of the data in the parameter domain and the automatically generated RWF, whose values vary between $\lambda = 10^{-4}$ (red) and $\lambda = 5.6 \cdot 10^{-6}$ (dark blue). Note that adaptation algorithm ensures low values of the RWF near the leading edge of the blade (which corresponds to a centrally located vertical line in the domain), while the values in the feature region (which is located in the southwest corner of the domain) remain unchanged.

The approximations results are visualized in Figure 11:
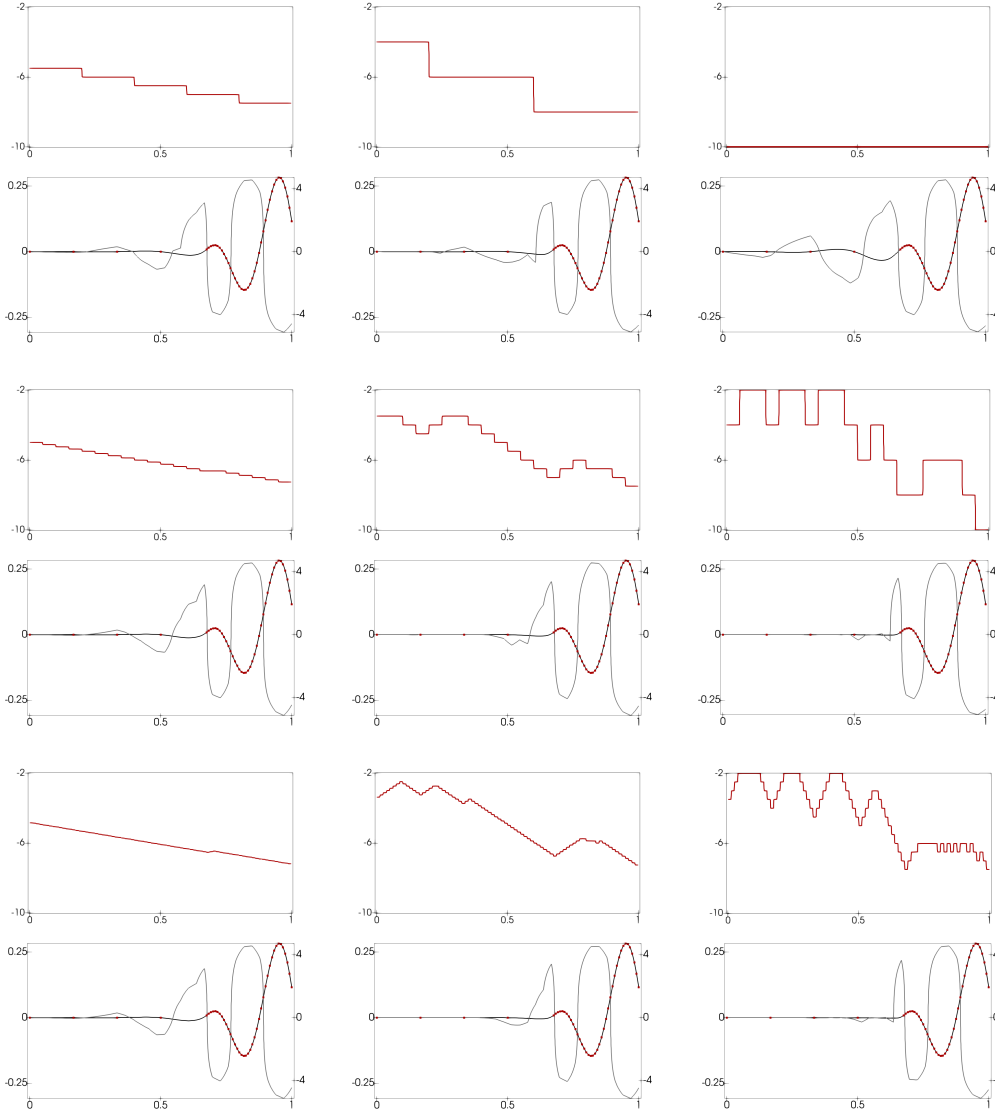
Fig. 9 RWFs (red curves), approximations (black curves) and signed logarithm (grey curves) of the second derivatives generated by the error–guided adaptation algorithm, for $\alpha \in \{10^{-2.5}, 10^{-10}, 10^{-40}\}$ (from left to right) and $k \in \{\frac{1}{5}, \frac{1}{20}, \frac{1}{80}\}$ (from top to bottom)

- For the larger constant RWF (top row), $\lambda = 10^{-4}$, we observe no oscillations near the feature of the blade, but we get a relatively high maximum error of $2.05 \cdot 10^{-4}$. Only 77% of the points satisfy the required tolerance $5 \cdot 10^{-5}$.
- For the smaller constant RWF (middle row), $\lambda = 10^{-6}$, we observe significant oscillations near the feature, but we obtain a lower maximum error of $4.13 \cdot$
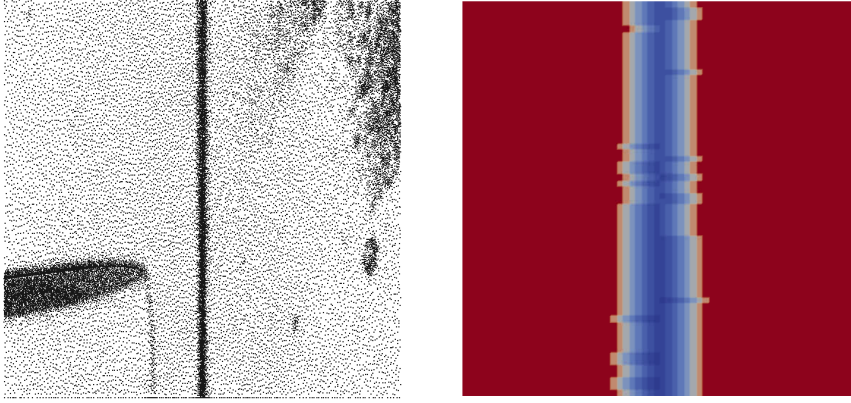
Fig. 10 Data (left) and the automatically generated adaptive RWF λ (right), both on the parameter domain of the blade surface.

10^{-5}. Now, all the points are below the tolerance, but the surface quality is insufficient.
– Finally, the approximation with adaptively constructed λ (bottom) combines high surface quality (no oscillations) with a low maximum error of $4.97 \cdot 10^{-5}$. Again, all the points satisfy the required tolerance.

4 Conclusion

We explored the use of a non-constant regularization weight function for least-squares tensor-product spline fitting. First, we analyzed the effect of introducing a regularization term for least-squares fitting in the context of data with holes. We established conditions on the RWF, in particular on its behaviours near to the hole's boundaries, that ensure the optimal rate of convergence.

Second, we presented two methods for automatically generating non-constant RWFs that are adapted to the data. The first one, which we called the support-guided RWF, was shown to be particularly well suited for data with holes. The second method, which uses an iterative procedure to adapt the RWF to the data, is useful when features are present in the data.

Besides the issue of stabilization, which was already mentioned in Section 2.2, the possible future work may aim at extending the theoretical results to the discrete case. Moreover, the regularization concepts for tensor-product spline surfaces can be further advanced by the study of more flexible RWFs and their construction. So far, only tensor-product splines were used as RWFs, thereby imposing limitations on the shape of the support boundaries. Additional flexibility may be useful when dealing with holes of general shape, and possibilities for adaptive refinement (cf. Giannelli et al. (2014)) are potentially beneficial as well.
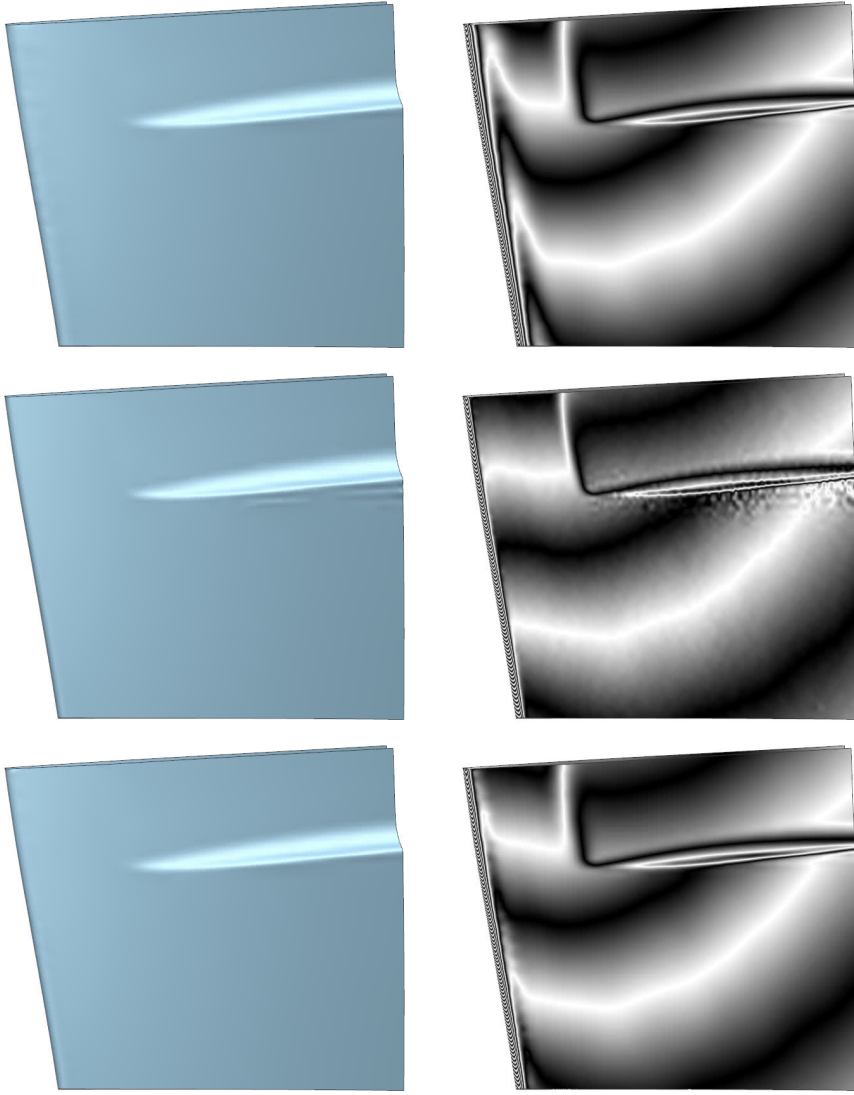
Fig. 11 The three approximations (surfaces and reflection line visualization) of a turbine blade. Top: $\lambda = 10^{-4}$, center: $\lambda = 10^{-6}$, bottom: adaptive λ.

Appendix: A bound on the Sobolev seminorm of the truncated spline projection

The proof of Theorem 1 relies on a bound on the Sobolev seminorm of the truncated spline projection. We use this appendix to present this result, together with its proof.

Proposition 1 *We consider again the assumptions of Theorem 1. The truncated spline projection defined in* (5) *satisfies*

$$|u_h|^2_{W^{2,2}(\Omega),\lambda} \leq \varepsilon C_3 h^{2p+2} \; ,$$

where the constant C_3 depends on f, ω, p and q.

Before presenting the proof, we derive an auxiliary result.

Lemma 3 *Given a point $\mathbf{t}_0 \in [0,1]^d$, we consider multi-indices $\mathbf{i}_h$ satisfying*

$$\mathbf{t}_0 \in \operatorname{supp} B^p_{\mathbf{i}_h,h}$$

that are indexed by a zero sequence of mesh sizes h. The values of the associated linear coefficient functionals converge to the value of the function at this point,

$$\lim_{h \to 0} \mu^p_{\mathbf{i}_h,h}(\phi) = \phi(\mathbf{t}_0)$$

if ϕ is C^2 smooth.

Proof For each mesh size h we denote with Δ_h the d-dimensional knot span that contains $\mathbf{t}_0$ (or one of them, if several knot spans with this property exist). As the first step, we exploit the linearity of the coefficient functionals and the equivalence of the norms on the finite-dimensional space of polynomials of degree p to conclude that

$$\max_{\mathbf{i}:\Delta_h \subseteq \operatorname{supp} B^p_{\mathbf{i},h}} |\mu^p_{\mathbf{i},h}(\phi) - \phi(\mathbf{t}_0)| = \max_{\mathbf{i}:\Delta_h \subseteq \operatorname{supp} B^p_{\mathbf{i},h}} |\mu^p_{\mathbf{i},h}(\phi - \phi(\mathbf{t}_0))|$$

$$\leq \frac{C_9}{h^d} \Big\| \sum_{0 \leq \mathbf{i} \leq \mathbf{m}_h + p} B^p_{\mathbf{i},h}(\mathbf{t}) \mu^p_{\mathbf{i},h}(\phi - \phi(\mathbf{t}_0)) \Big\|_{L^2(\Delta_h)} = \frac{C_9}{h^d} \Big\| \Pi^p_h(\phi) - \phi(\mathbf{t}_0) \Big\|_{L^2(\Delta_h)} ,$$

where the existence of the h-independent constant C_9 is guaranteed by the quasi–uniformity of the knot vectors. The factor $1/h^d$ is due to the integration over the knot span that is involved on the definition of the L^2 norm on Δ_h. Secondly we apply the triangle inequality, arriving at

$$\Big\| \Pi^p_h(\phi) - \phi(\mathbf{t}_0) \Big\|_{L^2(\Delta_h)} \leq \Big\| \Pi^p_h(\phi) - \phi \Big\|_{L^2(\Delta_h)} + \Big\| \phi - \phi(\mathbf{t}_0) \Big\|_{L^2(\Delta_h)} .$$

While we may use the inequality (2) with $\ell = p$ and domain Δ_h to bound the first term on the right–hand side, the second term can be estimated via the first derivatives, which gives

$$|\phi(\mathbf{t}) - \phi(\mathbf{t}_0)| \leq |h \max_{\mathbf{t}' \in \Delta_h} \|\nabla\phi(\mathbf{t}')\| | \quad \text{if} \quad \mathbf{t} \in \Delta_h$$

since ϕ is required to be C^2 smooth. Finally we complete the proof by combining these observations to obtain

$$|\mu^p_{\mathbf{i}_h,h}(\phi) - \phi(\mathbf{t}_0)| \leq \max_{\mathbf{i}:\Delta_h \subseteq \operatorname{supp} B^p_{\mathbf{i},h}} |\mu^p_{\mathbf{i},h}(\phi) - \phi(\mathbf{t}_0)|$$

$$\leq \frac{C_9}{h^d} \Big(C_1 h \underbrace{|\phi|_{W^{1,2}(\Delta_h)}}_{\leq C_{11} h^d |\phi|_{W^{2,\infty}(\Omega)}} + C_{10} h^{d+1} |\nabla\phi|_{W^{1,\infty}(\Omega)} \Big)$$
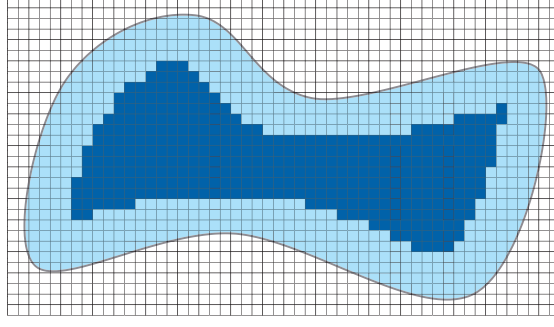
and noting that the right-hand side converges to zero as $h \to 0$. $\qquad\square$

Now we are ready to prove the proposition.

Proof (Proposition 1) Let

$$H^s = \Omega \setminus \bigcup_{\mathbf{i}:\, \omega B^{\mathbf{P}}_{\mathbf{i},h} \neq 0} \operatorname{supp} B^{\mathbf{P}}_{\mathbf{i},h} \subset H$$

be the subdomain of Ω with the property that no basis function possesses a support which simultaneously overlaps Ω_0 and H^s, see Figure 12.

Fig. 12 A domain Ω, a subdomain H (hole, light and dark blue) and the resulting subdomain H^s (dark blue), for $p = 3$

We split the domain into several subdomains and obtain

$$|u_h|^2_{W^{2,2}(\Omega),\lambda} = \int_\Omega \lambda(\mathbf{t}) \sum_{\nu,\eta=1}^d \left((\partial_{\nu\eta} u_h(\mathbf{t}))\right)^2 d\mathbf{t}$$

$$= \underbrace{\int_{\Omega_0} \lambda \sum_{\nu,\eta=1}^d (\partial_{\nu\eta} u_h)^2 d\mathbf{t}}_{(a)} + \underbrace{\int_{H\setminus H^s} \lambda \sum_{\nu,\eta=1}^d (\partial_{\nu\eta} u_h)^2 d\mathbf{t}}_{(b)} + \underbrace{\int_{H^s} \lambda \sum_{\nu,\eta=1}^d (\partial_{\nu\eta} u_h)^2 d\mathbf{t}}_{(c)} .$$

We note that $\lambda|_{\Omega_0} = 0$, thus the integral (a) does not contribute to the squared L^2 norm. Similarly, the integral (c) also vanishes since $T_h^p(\Pi_h^p f)|_{H^s} = 0$. The integral (b) can be estimated by

$$\int_{H\setminus H^s} \lambda \sum_{\nu,\eta=1}^d (\partial_{\nu\eta} u_h)^2 d\mathbf{t} = \int_{H\setminus H^s} \lambda \sum_{\nu,\eta=1}^d (\partial_{\nu\eta} T_h^p \Pi_h^p f)^2 d\mathbf{t}$$

$$\leq \int_{H\setminus H^s} \lambda \sum_{\nu,\eta=1}^d \sum_{\substack{\mathbf{i}:\, 0\leq\mathbf{i}\leq\mathbf{m}_h+p \\ \mathbf{j}:\, 0\leq\mathbf{j}\leq\mathbf{m}_h+p \\ B_{\mathbf{i},h}^p \cdot B_{\mathbf{j},h}^p|_{H\setminus H^s}\neq 0}} |\mu_{\mathbf{i},h}^p(f)\mu_{\mathbf{j},h}^p(f)| \, |\partial_{\nu\eta} B_{\mathbf{i},h}^p \partial_{\nu\eta} B_{\mathbf{j},h}^p| \, d\mathbf{t} .$$

According to Lemma 3 there exists a constant C_4 – which depends on f – such that the coefficient functionals satisfy $|\mu_{\mathbf{i},h}^{\mathbf{P}}(f)| \leq C_4$ if the value of h is sufficiently small, hence

$$\int_{H\setminus H^s} \lambda \sum_{\nu,\eta=1}^d (\partial_{\nu\eta} u_h)^2 d\mathbf{t} \leq C_4^2 \int_{H\setminus H^s} \lambda \sum_{\nu,\eta=1}^d \sum_{\substack{\mathbf{i}:\, 0\leq\mathbf{i}\leq\mathbf{m}_h+p \\ \mathbf{j}:\, 0\leq\mathbf{j}\leq\mathbf{m}_h+p \\ B_{\mathbf{i},h}^p \cdot B_{\mathbf{j},h}^p|_{H\setminus H^s}\neq 0}} (|\partial_{\nu\eta} B_{\mathbf{i},h}^{\mathbf{P}} \partial_{\nu\eta} B_{\mathbf{j},h}^{\mathbf{P}}|) d\mathbf{t} .$$

Moreover, for all ν, η, $\mathbf{i}$ and $\mathbf{j}$ there exists a constant C_5 such that

$$|\partial_{\nu\eta} B_{\mathbf{i},h}^p \partial_{\nu\eta} B_{\mathbf{j},h}^p| \leq C_5 h^{-4} ,$$

thus

$$\int_{H\setminus H^s} \lambda \sum_{\nu,\eta=1}^d (\partial_{\nu\eta} u_h)^2 d\mathbf{t} \leq C_4^2 C_5 h^{-4} \int_{H\setminus H^s} \lambda \sum_{\nu,\eta=1}^d \sum_{\substack{\mathbf{i}:\, 0\leq\mathbf{i}\leq\mathbf{m}_h+p \\ \mathbf{j}:\, 0\leq\mathbf{j}\leq\mathbf{m}_h+p \\ B_{\mathbf{i},h}^p \cdot B_{\mathbf{j},h}^p|_{H\setminus H^s}\neq 0}} 1 \, d\mathbf{t} .$$

The number of terms in the summation can be bounded by a constant multiplied with the number of elements that intersect $H \setminus H^s$, i.e., by $\frac{C_6}{h^{d-1}}$, where the constant C_6 depends on p, d and ω. We thus arrive at

$$\int\limits_{H \setminus H^s} \lambda \sum_{\nu,\eta=1}^{d} (\partial_{\nu\eta} u_h)^2 \mathrm{d}\mathbf{t} \leq C_4^2 C_5 C_6 h^{-d-3} \int\limits_{H \setminus H^s} \lambda \, \mathrm{d}\mathbf{t} \ .$$

We now use the assumption (4), which implies

$$\lambda(\mathbf{t}) \leq \varepsilon \operatorname{dist}(\mathbf{t}, \partial H)^q \leq \varepsilon C_7 h^q \text{ on } H \setminus H^s$$

and the fact that

$$\operatorname{vol}_d(H \setminus H^s) \leq C_8 h$$

to get

$$\int\limits_{H \setminus H^s} \lambda \, \mathrm{d}\mathbf{t} \leq \varepsilon C_7 C_8 h^{q+1} \ .$$

Finally we arrive at

$$\int\limits_{H \setminus H^s} \lambda \sum_{\nu,\eta=1}^{d} (\partial_{\nu\eta} u_h)^2 \mathrm{d}\mathbf{t} \leq \varepsilon C_4^2 C_5 C_6 C_7 C_8 h^{q-d-2} \ .$$

The claimed result then follows since $q \geq 2p + 4 + d$ is assumed in the theorem. $\qquad\square$

References

de Boor C, Fix G (1973) Spline approximation by quasiinterpolants. Journal of Approximation Theory 8(1):19–45

Bracco C, Giannelli C, Großmann D, Imperatore S, Mokriš D, Sestini A (2022) THB-spline approximations for turbine blade design with local B-spline approximations. In: Mathematical and Computational Methods for Modelling, Approximation and Simulation, Springer, pp 63–82

Carr JC, Beatson RK, Cherrie JB, Mitchell TJ, Fright WR, McCallum BC, Evans TR (2001) Reconstruction and representation of 3D objects with radial basis functions. In: Proc. 28th Annual Conference on Computer Graphics and Interactive Techniques (SIGGRAPH'01), pp 67–76

Chu BD, Martin F, Reif U (2022) Stabilization of spline bases by extension. Adv Comp Math 48:1–21

Deng C, Lin H (2014) Progressive and iterative approximation for least squares B-spline curve and surface fitting. Comput. Aided Des. 47:32–44

Floater MS, Hormann K (2005) Surface parameterization: a tutorial and survey. Advances in multiresolution for geometric modelling pp 157–186

Giannelli C, Jüttler B, Speleers H (2014) Strongly stable bases for adaptively refined multilevel spline spaces. Adv Comp Math 40:459–490

von Golitschek M, Schumaker LL (1990) Data fitting by penalized least squares. In: Algorithms for approximation II, Chapman and Hall, London, pp 210–227

Greiner G, Hormann K (1997) Interpolating and approximating scattered 3D-data with hierar-
    chical tensor product B-splines. In: Surface Fitting and Multiresolution Methods, Vanderbilt
    University Press, pp 163–172

Hoppe H, DeRose T, Duchamp T, Halstead M, Jin H, McDonald J, Schweitzer J, Stuetzle W
    (1994) Piecewise smooth surface reconstruction. In: Proceedings of the 21st annual confer-
    ence on Computer graphics and interactive techniques, pp 295–302

Hoschek J (1988) Intrinsic parametrization for approximation. Comput. Aided Geom. Des.
    5:27–31

Hoschek J, Jüttler B (1999) Techniques for fair and shape–preserving surface fitting with
    tensor–product B-splines. In: Shape Preserving Representations in Computer Aided Design
    (J.M. Peña, ed.), Nova Science publishers, New York, NY, pp 163–185

Hoschek J, Lasser D (1993) Fundamentals of computer aided geometric design. AK Peters,
    Ltd.

Jüttler B, Felis A (2002) Least-squares fitting of algebraic spline surfaces. Adv Comput Math
    17:135–152

Kiss G, Giannelli C, Zore U, Jüttler B, Großmann D, Barner J (2014) Adaptive CAD model
    (re-) construction with THB-splines. Graphical models 76(5):273–288

Piegl L, Tiller W (1996) The NURBS book. Springer Science & Business Media

von Golitschek M, Schumaker LL (2002) Penalized least squares fitting. Serdica Math J 28:329–
    348

Wang J, Yang Z, Jin L, Deng J, Chen F (2011) Parallel and adaptive surface reconstruction
    based on implicit PHT-splines. Comput. Aided Geom. Des. 28:463–474

Yang H, Wang W, Sun J (2004) Control point adjustment for B-spline curve approximation.
    Comput. Aided Des. 36(7):639–652